OTC 19332

Mechanisms by Which Methane Gas and Methane Hydrate Coexist In Ocean Sediments

Javad Behseresht, Yao Peng, Maša Prodanović, Steven L. Bryant, The University of Texas at Austin, Antone K. Jain and Ruben Juanes, Massachusetts Institute of Technology

Abstract

A spectrum of behavior is encountered in methane hydrate provinces, especially ocean sediments, ranging from essentially static accumulations where the pore space is filled with hydrate and brine, to active seeps where hydrate and methane gas phase co-exist in the hydrate stability zone (HSZ).

We present grain-scale models of drainage and fracturing, key processes involved in pressure-driven gas phase invasion of a sediment. A novel extension of invasion percolation to infinite-acting, physically representative networks is used to evaluate the connectivity of water in a gas-drained sediment. A novel implementation of the level set method (LSM) is used to determine the capillarity-controlled displacement of brine by gas from sediment and from fractures within the sediment. The discrete element method (DEM) is extended to model the coupling between the pore fluids and the solid and thereby predict the onset of sediment fracturing by gas phase pressure under in situ loading conditions. The DEM grain mechanics model accounts for the different pressure of brine and methane gas, in a "membrane" two-fluid model. The fluid-fluid configuration from LSM can be mapped directly to the pore space in DEM, thereby coupling the drainage and mechanics models. The type of behavior that can emerge from the coupled processes is illustrated with an extended LSM model. The extension computes grain displacement by the gas phase with a simple kinematic rule.

The LSM predicts gas/brine interface movement in sediment/fractures, and the DEM shows that the interface location affects the strength of sediment. Network simulations indicate that brine in drained sediment is better connected than previously believed. This increases the availability of water, water-gas interface area and consequently the rate of counter-diffusion of salinity ions, thus relaxing the limit on hydrate build-up within a gas-invaded region. The DEM model reproduces the key processes in the fluid-solid interaction. It was validated by means of isochoric pressurization tests, multistep inflow/outflow experiments, and drained/undrained consolidation tests. DEM simulations reproduce the sediment stress-strain behavior in laboratory triaxial experiments. The DEM model shows that vertical fracturing of the sediment is favored at the base of the hydrate stability zone. The kinematic extension of LSM yields much broader capillary pressure curves and self-reinforcing invasion paths, confirming the utility of ongoing efforts to integrate the DEM and network/LSM models.

Introduction

The mass of carbon held in sediments below the seafloor is a significant reservoir within the Earth's carbon cycle. The amount currently in place may be very large, enough to implicate methane hydrates in global warming events in the geological past and to raise the prospect of a vast energy resource. However, estimates of this mass and the rate at which it can accumulate in or dissipate from sediments vary widely. One reason is the difficulty in ascertaining form and spatial distribution of methane within the hydrate stability zone (HSZ).

The manner of transport of methane within the HSZ must influence the spatial distribution of hydrate, so a quantitative model of transport can yield useful insight. One possible mode of transport is single phase: water containing dissolved methane rises into the HSZ (Bhatnagar et al. 2007). Our focus is on a different mode: two-phase flow. This is motivated by the frequent (though not universal) observation of gas, water and hydrate phases co-existing within the HSZ. An extensive accumulation of gas phase below the HSZ is also observed or inferred in some hydrate provinces. Thus we have been led to propose the following hypothesis: the coupling between geomechanics, the dynamics of gas/water interfaces, and phase

behavior of the gas/brine/hydrate system make co-existence of free gas and hydrate inevitable in the HSZ. We are developing mechanistic models to elucidate the coupled behavior.

Several phenomena must play a role in any sediment in which hydrate is forming as a result of gas and brine phases coming into contact. One phenomenon is capillarity. The geometry of an interface between two fluid phases in a sediment is controlled by capillary forces. The interface is not a single uninterrupted entity; at the grain scale it occupies many individual pore throats simultaneously. Because gas and water movement are often driven by episodic forcing events, capillary hysteresis is inevitable. Consequently, the distribution of fluid phases within sediment, and hence the distribution of hydrate, will be a complicated function of the forcing events and the grain-scale structure of the sediments.

A second key process is unsaturated sediment mechanics, that is, the mechanical behavior of the sediment in the presence of several fluid and solid phases in the pore space (water, gas and hydrate). While capillarity governs invasion of gas through the porous medium, mechanical effects may lead to deformation and fracturing of the sediment skeleton, thereby triggering invasion when it would otherwise not occur. Methane invasion by fracture opening is common, as evidenced by field observations of tensile fractures at the seafloor and hydrate layers along bedding planes. The fracturing pressure in this application is exerted by a gas phase. The gas pressure acts upon the non-wetted surfaces of the sediment grains. Moreover, the water held at grain contacts as pendular rings increases the cohesion of the sediment (Orr et al., 1975; Lian et al., 1993; Willett et al., 2000), which in turn affects the mechanical response. These processes clearly couple flow and deformation, at both the grain scale and the macroscopic scale.

In this paper we describe mechanistic grain-scale models for the capillarity-controlled displacement of brine by gas. The implications of model predictions for water and gas availability for hydrate formation are discussed. We also describe mechanistic grain-scale model for the displacement of sediment grains. The qualitative effect of coupling the two models is also presented.

In the remainder of the Introduction we give an overview of the techniques being applied.

Grain-scale Description of Sediments. We use densely packed, randomly arranged spheres with prescribed grain size distributions as model sediments. All sphere coordinates and radii are known. The spheres are packed in a periodic unit cell to eliminate edge effects. Figure 1a shows a small sample. Knowledge of the sphere centers permits an unambiguous characterization of the pore space using Delaunay tessellation (Bryant et al. 1993, Al-Raoush et al. 2003). Delaunay tessellation subdivides the pore space into a set of tetrahedra whose vertices are the coordinates of the sphere centers. Figure 1b shows a Delaunay cell defined by four equal spheres. The faces of a cell correspond to pore throats because pore space is narrowest there. Each pore generated with Delaunay tessellation has four neighbors, and thus the network of pores has a uniform coordination number of four.

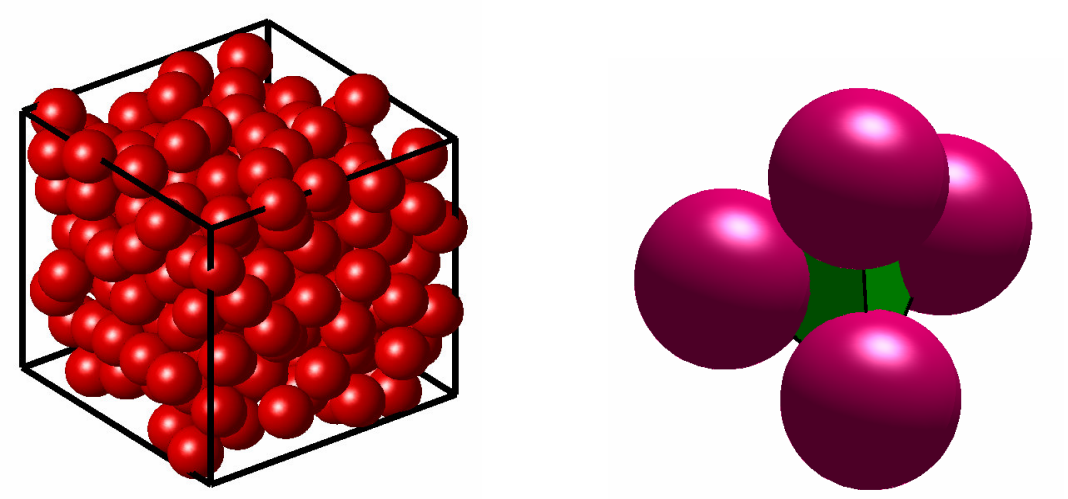

(a) (b)

Figure 1. (a) A sample sphere packing in a until cell. (b) A Delaunay cell formed by four neighboring spheres' centers. A Delaunay pore is the pore space within the tetrahedron and outside the spheres. Tetrahedron sides (shown in green) define throats controlling access to the pore.

Drainage of water by gas depends on the geometry of the pore throats in the sediment. We account for this by assigning a critical curvature to the throats. Critical curvature is defined as the minimum curvature of the meniscus needed for nonwetting phase displace wetting phase from the pore throat. For simplicity we use the Haines inscribed sphere curvature with the correction from Mason and Mellor (1995):

$$C = \frac{2R_{avg}}{r_{inscribed}} - 1.6 \tag{1}$$

In the above equation, R_{avg} is the average sphere radius in the model sediment, and $r_{inscribed}$ is the radius of the inscribed sphere in a throat. The correction of −1.6 provides good agreement with the Mayer-Stowe-Princen estimate of critical curvature (Mayer and Stowe 1965; Princen 1969a, 1969b, 1970).

In load-bearing sediments many pairs of grains are in contact. After pores surrounding a grain contact have drained, wetting phase remains as a pendular ring held at the contact. In many granular materials, and in the sphere packings used here, some grains are separated by narrow gaps, at which a liquid bridge of wetting phase can remain after nearby pores have drained. The volumes of these rings and bridges are small, but their role in connecting not-yet-drained pores is important (Behseresht et al., 2007). Because our network representation of the sediment pore space is derived from the sediment grain locations, it is relatively easy to extend the network data structure to account for rings and bridges. This would be difficult with traditional networks, which account only for pore bodies and pore throats.

Network Models of Capillarity-Controlled Displacements. The network model introduced by Fatt (1956a,b,c) joins tubes of different diameters at the intersection points on regular lattices. The topology of pore space in sediments is not regular, and it is not possible to obtain the distribution of tube diameters without performing a capillary pressure experiment. Physically representative networks circumvent these limitations by construction directly from the geometry of grain space in the sediment (Bryant et al. 1993). We use the Delaunay tessellation described above for this construction. Modifications (Al-Raoush et al. 2003) of the Delaunay tessellation eliminate pathological cells (typically, pores in regions of larger-than-average porosity), but yield networks with nonuniform connectivity. The features of interest in this work (distribution and connectivity of wetting phase) are not sensitive to these modifications, so the simpler Delaunay construction is adequate.

We have extended this network construction to handle the periodic boundaries of the model sediments (Behseresht et al. 2007). This eliminates boundary effects from the drainage simulations. We summarize the approach below, and use it to quantify the connectivity of the wetting phase at various stages of drainage. This is a key measure of water availability for hydrate formation at the gas-water interface.

Level Set Methods for Capillarity-Controlled Fluid Displacements with Stationary Grains. Network models are a useful way of upscaling pore-level information to obtain macroscopic behavior. However, idealizations are necessary to make these models tractable. Since the geometry of menisci obeying the Young-Laplace equation is central to capillary displacement, we are interested in methods that better resolve the motion of menisci. The level set method is ideally suited for this purpose (Sethian 1999; Osher and Fedkiw 2001). In this method, the meniscus is the zero level set of a function $\phi(\vec{x}, t)$. That is, the location of the meniscus at any time t is the set of points x where $\phi(\vec{x}, t) = 0$. The function evolves in time according to the following PDE:

$$\phi_t + F|\nabla\phi| = 0, \quad \phi(\vec{x}, 0)\ given \tag{2}$$

where F is speed of the meniscus in the direction normal to itself.

The power of the method stems from the fact that the meniscus is embedded in the level set function defined on the entire domain. This eliminates the necessity of explicitly tracking each point on the meniscus separately. As a result, the method requires no special treatment of topology changes (disconnection or reconnection of fluid volumes). Such changes are ubiquitous in capillarity-controlled displacements. Examples include Haines jumps from one throat into many; withdrawal of nonwetting phase from multiple pore throats into a single throat and snap-off of nonwetting phase in a single throat.

We have specialized the method by associating the speed function with the balance between capillary pressure forces and interfacial tension, as described below. We also introduce an auxiliary level set function $\psi(\vec{x})$ which defines the location of solid grains: $\psi(\vec{x}) > 0$ for locations $\vec{x}$ inside a grain and $\psi(\vec{x}) < 0$ for locations $\vec{x}$ within pore space. This permits application of the same code to model sediments (this paper) and to high-resolution digital images such as X-ray micro-computed tomography images of real materials (Prodanović and Bryant 2007, 2008).

Discrete Element Methods for Grain Poromechanics with Single Fluid Phase. The Discrete Element Method (DEM) (Cundall and Strack 1979) has proved a valuable tool to study the mechanisms for deformation and failure of granular materials with variable degree of cementation (Bruno and Nelson 1991). Moreover, based on simple geometric arguments, stress variations (and subsequent deformation) have been shown to affect flow properties such as porosity and permeability (Bruno 1994).

In DEM, each element or grain is identified separately by its own mass, moment of inertia and contact properties. For each grain, its translational and rotational movements are described by solving Newton's second law of motion. The movement of a grain is dictated by the net force and moment acting on it. For a dry model, that is, one in which pore pressures are negligible, the forces acting on each grain are restricted to grain-grain interactions.

When the pore space is filled with a single fluid phase at non-negligible pressure, the associated forces must be incorporated in the model. A conceptual view of the new set of forces is shown in Figure 2. We used the commercial code PFC2D (Itasca, 2005) as a platform to develop a coupled model with rigorous two-way coupling: (1) The pore fluid pressure

exerts forces on solid grains, contributing to the deformation of the medium; (2) Grain rearrangements cause changes in volume of individual pores which, in turn, yield pore-pressure changes. Moreover, the hydraulic of the medium will change as a result of deformation. Notably, this is reflected in the dependence of the pore-to-pore conductance on the distance between grains.

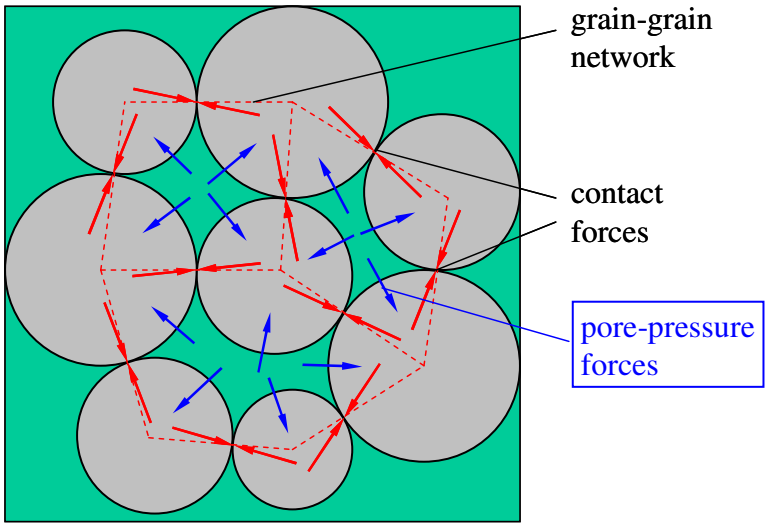

Figure 2. Conceptual picture of the fluid-solid interaction model at the pore scale when a single fluid is present.

Discrete Element Methods for Grain Poromechanics with Two Fluid Phases. In the environments of interest for methane hydrates—in particular, at the base of the hydrate stability zone—two fluid phases exist: a liquid brine phase, and methane gas. One of the key differences between single fluid and two fluid systems is the presence of a fluid-fluid interface. Due to surface tension effects, the pressures on both sides of the interface (that is, the pressure of brine and the pressure of methane gas) can be very different. This pressure difference may lead to preferential fracturing of the sediment. While this is typically not a favored scenario in single-fluid systems, it is natural in two-fluid systems.

Here, we adopt an "elastic membrane" representation of the gas/water interface that only allows normal forces to be transmitted. Adhesion forces are neglected at this stage. When the bond between two grains is lost, the "membrane" advances and a new pore is loaded with a higher pressure. A simple and elegant formulation of the key hydraulic property (the conductance between pore bodies) has recently allowed us to consider such processes. The basis is to allow flow (that is, have a positive conductance between two pores) only when the bond between grains is broken, and a gap of sufficient width has been formed. The implementation details are described in the Methods section.

Level Set Methods for Capillarity-Controlled Fluid Displacements with Movable Grains. The grain space level set $\psi(\vec{x})$ offers a convenient data structure for tracking the location of grains displaced by fluid pressure. Thus as an adjunct to the DEM model, we have also implemented a proof of concept calculation of drainage coupled with grain displacement. For this purpose a kinematic (rather than mechanistic) treatment of the grain movement using the elastic membrane concept is sufficient. These calculations indicate the range of behaviors that could emerge from the coupling and provide preliminary insight into the mechanically rigorous calculations. The key point is that capillarity-controlled invasion localizes the force exerted by the gas phase to grains along the gas/water interface. Grain displacement alters the critical curvature of throats associated with those grains, thus affecting subsequent drainage events. This feedback loop creates patterns in the displacement that do not exist for uncoupled processes.

Methods

Model Sediments. We use the cooperative rearrangement algorithm (Thane 2006), to create a set of densely packed, randomly arranged spheres. The size distribution of the spheres varies from monodisperse to moderately well sorted. We quantify sorting with the Trask coefficient, defined as $S_0 = \sqrt{d_{75}/d_{25}}$, where d is grain diameter and the subscript indicates the corresponding position in the cumulative grain size distribution function, in percent. The unit cell in which the spheres are packed is periodic, so edge effects (locally ordered arrangements of spheres) do not arise. The model sediments used here contain 5000 to 7000 spheres. These are good models of the grain- and pore-space geometry in naturally occurring sand-rich deposits. They are not directly applicable in their current form to clay-rich sediments, though many of the insights gained from studying coupled phenomena in the sand-rich model should still be relevant.

Drainage in Infinite-acting Physically Representative Networks. From the known geometry of the periodic model sediments, we extract a network of pores that preserves periodicity. Figure 3 ilustrates the periodicity of the pores in one coordinate direction. Because the spheres are randomly arranged, the Delaunay tessellations are topologically random. Thus the periodicity is not trivial, as inspection of Figure 3 shows. We refer to these networks as "infinite-acting" because there is no natural choice of "outlet pores" for the displaced water phase. Instead, the notion of outlets is replaced by concepts from percolation theory, described below.

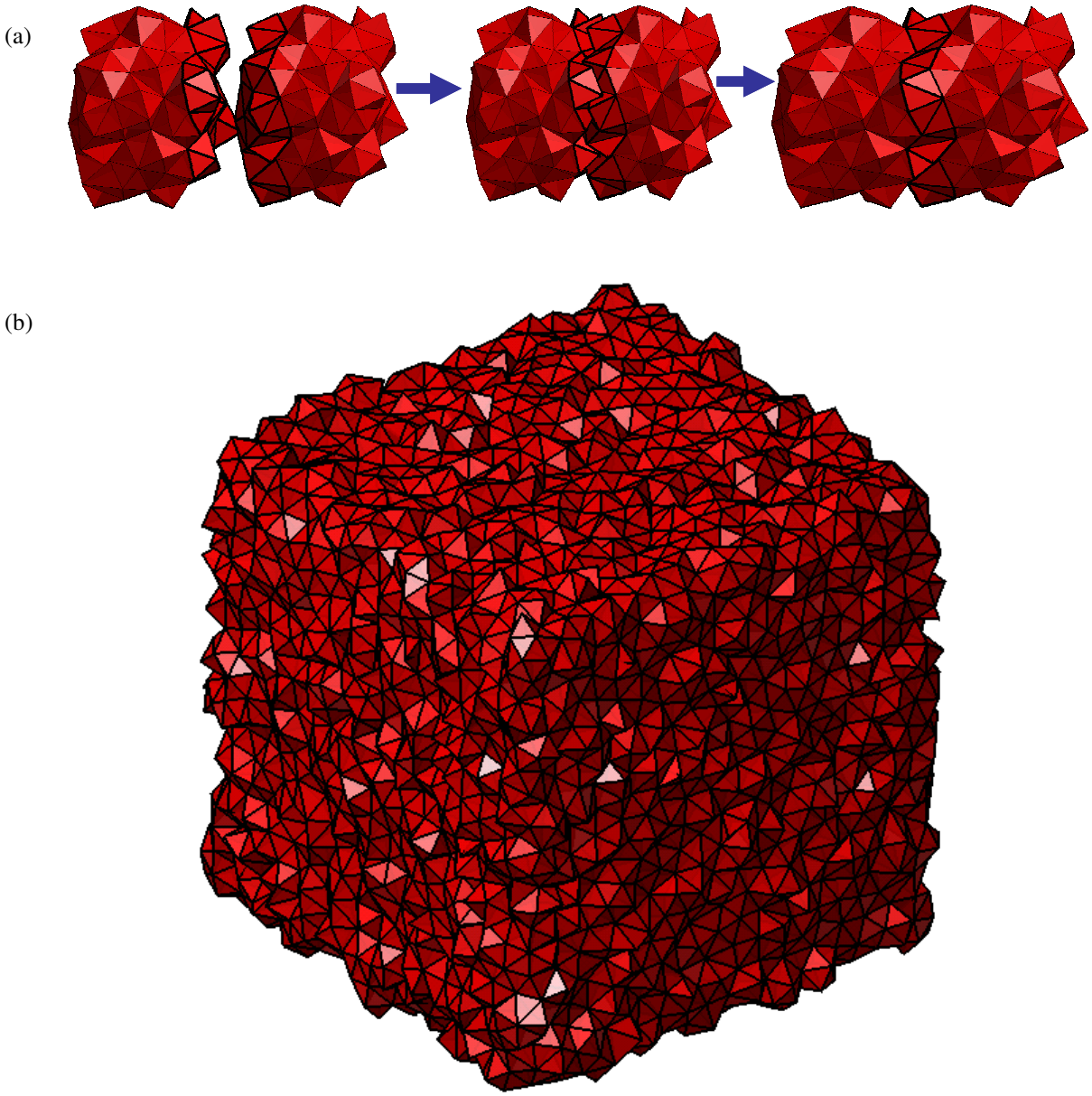

Figure 3. Periodicity in infinite-acting networks. (a) Delaunay tessellation of a periodic packing is also periodic, as illustrated with two replicas of a small sample. The sequence shows Delaunay tetrahedra edges near the periodic boundary (outlined in black; right face of the left-hand replica, and left face of the right-hand replica) slightly separated, moved closer and matched together. (b) The Delaunay tessellation of a model sediment establishes a periodic unit cell that is repeated in all directions to form an infinite-acting network.

Drainage Algorithm. We simulate drainage with a standard invasion percolation algorithm, modified to allow for trapping of wetting phase. The governing rules are based on "candidates" for drainage. A pore is a candidate for being drained only if it has at least one neighboring pore which is already empty of wetting phase (Mason and Mellor, 1995). A candidate may be drained from its already-drained neighbor if the current applied curvature exceeds the critical curvature of the throat connecting the pore to its already-drained neighbor. A candidate that meets the critical curvature test is allowed to

drain only if there is a connected path of wetting phase through which the contents of the pore could be displaced. The nature of this connected path is described in the next section.

The simulation starts with the pore space full of wetting phase. We select a small number of pores at random as sources through which nonwetting phase can invade the pore space. The applied capillary pressure is increased in small increments. After each increment, the rules for drainage are applied iteratively until no more candidates can be invaded at the current curvature.

Wetting Phase Trapping. Wetting phase cannot be displaced from a pore unless there is some place for it to go. In a traditional finite network, "some place" means an exit from the network. An infinite-acting network has no boundaries and thus no obvious choices for exit pores. Instead we consider wetting phase to be displaceable from a pore if that pore is part of any periodically connected loop of the wetting phase. Such a loop wraps around the infinite-acting network to connect to itself. This means it forms a continuous path of the wetting phase that extends indefinitely in the repeating unit cells. This loop naturally corresponds to a percolating cluster of pores occupied by wetting phase. Wetting phase in a pore not connected to such a cluster is considered trapped (see Figures 5 and 6 in Behseresht et al. 2007). The concept of a percolation threshold is general, and to the extent that the infinite-acting networks can capture this threshold correctly, they should provide a more realistic prediction of wetting phase configurations in nature.

Wetting Phase Connectivity. The existence of a connected path of wetting phase spanning the network is crucial to the trapping/displacement calculation. Thus the definition of "connected" is fundamental to our simulations. Traditional networks consider connectivity of fluids only through pore throats, the "bonds" in the lattice. In sediments, the wetting phase can occupy partially-formed pendular rings at grain contacts when one or two pores associated with the grain contact have drained. When all the pores associated with the contact have drained, the pendular ring is fully formed and is disconnected from the rest of the wetting phase. These partial rings establish a second type of connections between pores containing wetting phase. Under typical experimental conditions, wetting phase is displaced through the partially formed rings as well as through throats; otherwise, irreducible wetting phase saturations would be much larger than observed (Behseresht et al. 2007).

Pendular rings occur at grain contacts, which are associated with the edges of the Delaunay tetrahedra. The tetrahedra define the pores, so it is straightforward to associate each pendular ring with the appropriate pores. At each step of drainage, we identify individual clusters of pores containing wetting phase that are connected by throats containing wetting phase and/or by partial pendular rings. Each cluster is tested to determine whether it percolates, i.e. whether it spans the domain by means of periodic connections.

Level Set Method (LSM) for Interface Tracking: the Progressive Quasi-Static (PQS) Algorithm. When driven by slow changes in capillary pressure, immiscible displacement can be modeled as a quasi-static, capillarity-controlled process. Thus fluid interfaces at each stage of displacement are constant mean curvature (κ_M) surfaces, satisfying Young-Laplace equation $P_c = P_{nw} - P_w = 2\sigma\kappa_M = \sigma\kappa$ where *nw* and *w* denote non-wetting and wetting phases respectively, P_c is capillary pressure and σ is interfacial tension. For convenience in this work we assume perfectly wetted grains, so that the contact angle is not needed (assumed zero).

We have developed a simple but robust model for simulating both drainage and imbibition in general porous media assuming capillary forces are dominant (Prodanović and Bryant 2006, 2007, 2008). We are applying this method to evaluate the critical curvatures for drainage in pore throats in model sediments; this will test the validity of approximation of Eq. (1). In this paper we use the method to simulate displacement directly (i.e. with no geometry simplifications made), in small subsets of model sediments.

In drainage simulations, the algorithm first places a planar or circular interface near the entry of the computational domain. The interface is propagated with the slightly compressible velocity model, which defines the speed *F* in the evolution Eq. (2) as

$$F(\vec{x},t) = a_0 exp[K(1 - \frac{V(t)}{V_m})] - b_0\kappa(\vec{x},t) \tag{3}$$

The first term on the right hand side behaves like a capillary pressure, with prescribed pressure value a_0, target volume V_m and bulk-modulus f, and $V(t)$ is the non-wetting phase volume. The second term represents surface tension, with b_0 corresponding to interfacial tension, and $\kappa(\vec{x},t)$ is (twice) the mean curvature. With this speed function we integrate Eq. (1) in time until a steady state ϕ_I with the corresponding pressure a_I is reached. At steady state, the speed *F* is everywhere zero. Eq. (3) shows that the physical situation at steady state corresponds to a balance between capillary pressure and interfacial tension, i.e. the Young-Laplace equation.

The PQS algorithm consists of a series of steps. At each step beyond the initial one computed by the compressible model given in Eq. (1), we increase curvature by $\Delta\kappa$ (which is equivalent to incrementing capillary pressure by $\Delta a = b_0\Delta\kappa$), and run the prescribed curvature model

$$F(\vec{x},t) = a_0 - b_0\kappa(\vec{x},t) \tag{4}$$

until a new steady state is obtained. At steady state, Eq. (4), like Eq. (3), is a balance between capillary forces and pressure forces. After each step is computed, one can evaluate volume of the fluid, interfacial areas of interest, number of disconnected fluid components as well as any topological changes. Such changes might indicate some critical pore level events such as Haines jumps in throats during drainage or imbibition of a (set of) pore(s).

In the PQS algorithm we impose a constraint of the type $\phi(\vec{x},t) \leq \psi(\vec{x})$ after every iteration, where ψ is a fixed level set function whose zero level set is pore-grain boundary surface. This is an inexpensive numerical boundary condition that prevents the interface from entering grain space and results in a zero contact angle. We have implemented the PQS algorithm using standard approaches. Level Set Method Library (Chu and Prodanović, LSMLIB) contains most of the required routines in C/C++/FORTRAN. More details on implementation can be found in (Prodanović and Bryant 2006, 2008).

DEM for Grain Poromechanics with Single Fluid Phase. In DEM, each element or grain is identified separately by its own mass, moment of inertia and contact properties. The translational and rotational movements of each grain are described by solving Newton's second law of motion. The movement of a grain is dictated by the net force and moment acting on it. For a dry model, that is, one in which pore pressures are negligible, the forces for each grain may include: (1) contact force F_c due to the deformation at the grain contacts, (2) damping forces F_d due to grain non-elastic collisions; (3) external forces F_b due to gravity and prescribed tractions at the boundaries. The contact force F_c can be further split into normal and tangential components, F_c^n and F_c^t, respectively. Bulk behavior of a granular system is determined by all individual grain–grain interactions. For the analysis of dry samples, that is, systems in which the pore pressure is negligible, the interactions between particles can be associated with a network of grain–grain contact forces that connects the centroids of grains that are in contact.

Given the set of forces $\vec{F}_j$ and moments $\vec{M}_j$ acting on the *i*th particle, its motion is described by the following equations:

$$m_i\ddot{\vec{x}}_i = \sum_j \vec{F}_j, \quad I_i\ddot{\vec{\theta}}_i = \sum_j \vec{M}_j \tag{5}$$

Here, $\vec{x}_j$ and $\vec{\theta}_j$ are the position vector of the grain centroid and the angle vector of rotation about the centroid, respectively; the double dot symbols denote second time derivatives of the position and rotation angle; and m and I are the mass and moment of inertia, respectively. The equations of motion must be solved simultaneously for all grains in the system via a numerical integration scheme. A commercial DEM code, PFC2D/3D (Itasca, 2005), has been used.

From the theory of poromechanics (Biot 1941), it is well known that pore pressure will influence mechanical behavior. Essentially, compressive stresses in granular media are transmitted both through a solid skeleton and the pore fluids. Recently, models have been developed to incorporate this effect in DEM with a single-phase pore fluid (Shimizu 2004; Cook et al. 2004; Li and Holt 2006).

In addition to grain contact forces, the model must include the effect of the pore fluid (Figure 2). Computationally, the model then consists of two overlapping and interacting networks: the grain network and the fluid network. A particular instance is shown in Figure 4. The force that the fluid in one of the domains exerts on a particular grain is obtained by integrating the pressure along the contact area.

Consider one particular fluid domain, as sketched in Figure 5. The micromechanical equations can be summarized as follows. The flow rate out of the fluid domain through a pore throat is

$$q_j = \kappa a^2 \frac{p - p_j}{L_j}, \quad \kappa = \frac{kr}{a^2\mu}, \tag{6}$$

where κ is a conductance, a is an effective throat aperture, and L is an effective distance between pore centers. The conductance κ is a prescribed constant (that is inversely proportional to the fluid viscosity), so that all variations in flow rate are due to changes in aperture and pressure gradient. The dimensions of the flow rate are L^2T^{-1} for a two-dimensional problem. The relation between the conductance κ and the permeability k is given by the second equation above. The grains have certain compressibility, and the radius of a spherical grain varies according to

$$r = r_0\left(1 - \frac{p}{3K_s}\right) \tag{7}$$

where r_0 is the initial radius (at zero fluid pressure), K_s is the bulk modulus of the solid grain, and p is the average of the pressure around the grain. Finally, mass balance over a fluid domain gives the following pressure evolution equation

$$\delta p = \frac{K_f}{V_p}\left(-\delta V_p - \sum_j q_j \delta t\right) \tag{8}$$

where K_f is the fluid bulk modulus, and δp is the pressure variation after a time step δt. The main feature of our model is the term $-\delta V_p$, which accounts for the change in volume of each pore caused by changes in grain locations. This term has been neglected in previous investigations of pore-scale poromechanical models but is essential, for example, to reproduce

pressurization of the fluid upon fast compaction. It also reflects the reverse coupling present in Biot's self-consistent theory of poroelasticity.

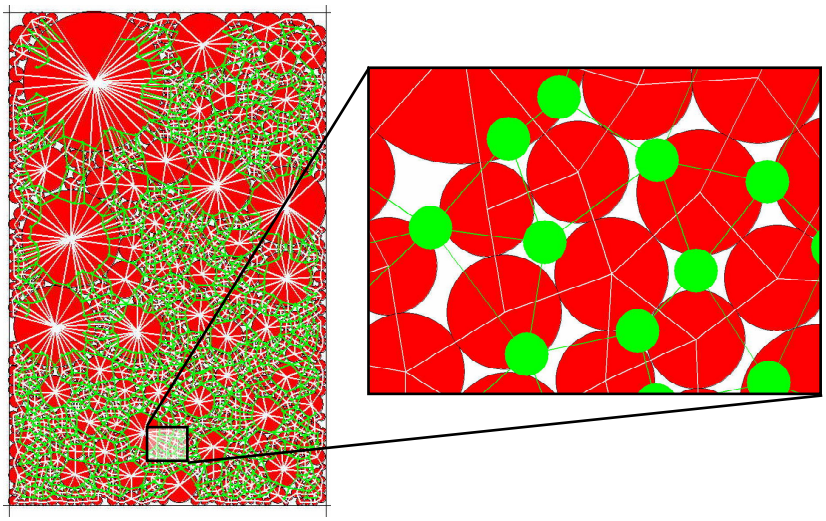

Figure 4. Representation (and zoom-in) of the grain (red) and fluid (green) networks.

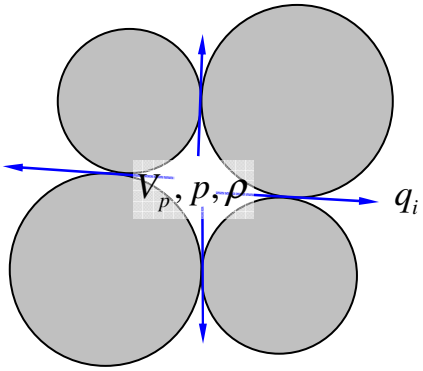

Figure 5. Schematic representation of a fluid domain. At any given time, each fluid domain is characterized by its pore volume V_p, and the pressure p and density ρ of the fluid. Fluid can go in and out of the pore domain at a rate q_i into the neighboring fluid domains.

DEM for Grain Poromechanics with Two Fluid Phases. Preferential fracturing of the sediment invariable requires differences in pressure between neighboring pores. While this is typically not a favored scenario in single-fluid systems (unless a fluid is injected at very fast flow rates and pressures, as in hydraulic fracturing operations), it is natural in two-fluid systems because the two fluids have different pressures. Because the two fluids do not mix, a pressure difference does not dissipate. This pressure difference may lead to preferential fracturing of the sediment.

Here, we adopt an "elastic membrane" representation of the gas/water interface that only allows normal forces to be transmitted. Adhesion forces are neglected at this stage. When the bond between two grains is lost, the "membrane" advances and a new pore is loaded with a higher pressure. In this fashion, the discontinuity in pressure between brine and gas can be maintained, while the gas advances through the network of pores.

This is done within the PFC code with a simple formulation of the key hydraulic property: the conductance between pore bodies. For the 2D simulations shown later, the apparent aperture of a pore throat is modeled as:

$$a = a_0 + f(d - d_0), \tag{9}$$

where d is the gap between grains, f is a multiplier, and a_0 reflects the effective hydraulic aperture when the gap between grains is zero. This expression can be readily generalized to 3D and captures the essential behavior. For homogeneous (single-phase) fluids, proper flow behavior requires that the first term be nonzero and, in most cases, dominant. This maintains hydraulic connectivity between pores which would otherwise be lost in 2D. The model thereby exhibits the correct diffusion of pressure in a single fluid phase.

In a two-fluid system, the difference in pressures between the fluids does not diffuse or equilibrate. In a quasi-static process, pressure changes can occur only if the fluid-fluid interface advances. We model this effect simply by selecting a very small value of a_0, a grain size-dependent value of d_0, and a value of $f = 1$. Thus the fluid-fluid interface will advance at an appreciable rate only when the aperture increases significantly from its initial value. While this is certainly a crude simplification of the conditions for capillary invasion of a throat, the model reflects the fact that the fluid-fluid interface will advance only when the capillary pressure exceed the capillary entry pressure (which requires that the gap be of a sufficient magnitude). The model, in turn, performs a rigorous calculation of the mechanical behavior of the sediment upon fluid migration.

PQS Fluid Displacement Coupled with Grain Displacement. PQS algorithm provides detailed knowledge of both fluid-fluid and fluid-solid interfaces. Furthermore, since we know the geometry of each individual grain we can isolate individual fluid-solid contacts. As a means of exploring the coupled behavior of meniscus movement and grain movement, we develop an approach complementary to the DEM for grain poromechanics with two fluid phases, with grain mechanics somewhat simplified, but with the advancing fluid-fluid interface computed rigorously. To simulate grain mechanics, we introduce the following steps after each PQS drainage step:

1) Identify grains in contact with non-wetting phase.

2) The non-wetting fluid (gas) exerts force, the vector sum of which we denote $\vec{F}_i$, on each grain *i* identified in step 1. Per the elastic membrane model, locally the force is normal to the fluid-grain contact (see Figure 6). To obtain $\vec{F}_i$, we integrate the normal vector $\vec{n}$ (pointing outwards from the gas phase) along the part Γ_{Gi} of the entire grain perimeter (surface) Γ_i in contact with gas. The then find the unit vector $\vec{f}_i$ in the same direction as $\vec{F}_i$.
3) Compute a displacement $\vec{s}_i$ in response to the force computed in step 2. The force is maximum when Γ_{Gi} is half-circle (half-sphere) so we set $\vec{s}_i = 4r(1-r)C\vec{f}_i$, where *r* is ratio of the lengths (areas) of Γ_{Gi} and of entire Γ_i, and *C* is a pre-set constant.
4) The center of grain i moves by $\vec{s}_i$ determined in step 3, but only if it will not overlap substantially with any other grains in its new position. By "substantially" in this work we mean that the distance between the grain centers would be less than 0.8 of the sum of their respective radii.

This conceptual procedure does not consider the forces imposed by neighboring grains, which are the essence of the solid mechanics; this is the proper role of DEM described above. Thus we do not attempt to determine the exact magnitude of F_i, nor the exact displacement $\vec{s}_i$ from Newton's 2nd law. The kinematic approach simply provides insight into the type of behavior that can arise from the coupled displacements.

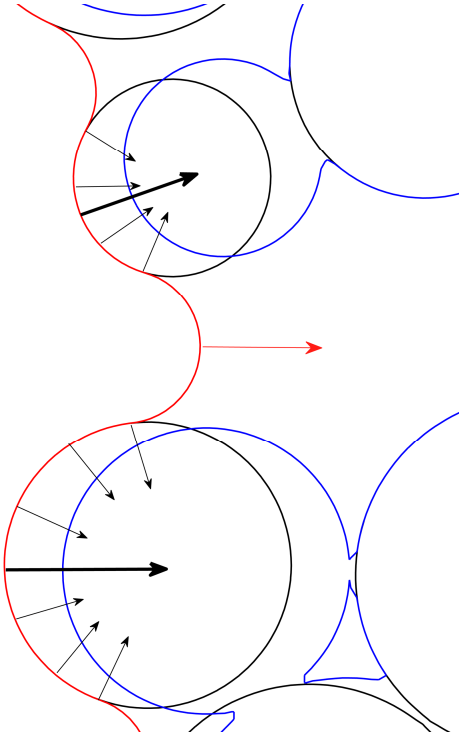

Figure 6. Sediment movement in case of two grains (this is isolated from the simulation show later in Results section, see Figure 24). Non-wetting fluid interface is shown in red and the initial grain position is shown in black. Small black arrows show the normal vectors along the on-wetting fluid-grain contact line and enlarged black arrows show their (integral) direction (and ultimately direction of the movement). New grain positions are outlined in blue.

Results

Effect of Sorting on Drainage Curve

Drainage simulations were conducted in infinite-acting networks for model sediments with several different grain size distributions. We plot drainage curves as dimensionless curvature vs. wetting phase saturation in Figure 7. The drainage curves vary systematically. The curvature at which percolation occurs (large increase in nonwetting phase saturation for small increment in curvature) decreases as the sorting becomes poorer. This is because the pore throat size distribution becomes wider as the grain size distribution becomes wider, assuming the mean grain size the same for all packings. The percolation threshold for drainage in these four-connected networks occurs when about 50% of the pore throats are occupied by nonwetting phase. As shown in Figure 8, this threshold occurs at larger pore throats in the wider pore throat size distributions. In pack 4, the 50% mark on the cumulative probability function occurs at $r_{throat}/R_{avg} = 0.28$. The dimensionless critical curvature to invade this throat is 5.6 (Eq. (1)), which is consistent with the drainage curve in Figure 7. Pack 57 has a larger proportion of large throats, and the threshold throat size is $r_{throat}/R_{avg} = 0.51$. The corresponding dimensionless critical curvature is 2.3, again consistent with the drainage curve.

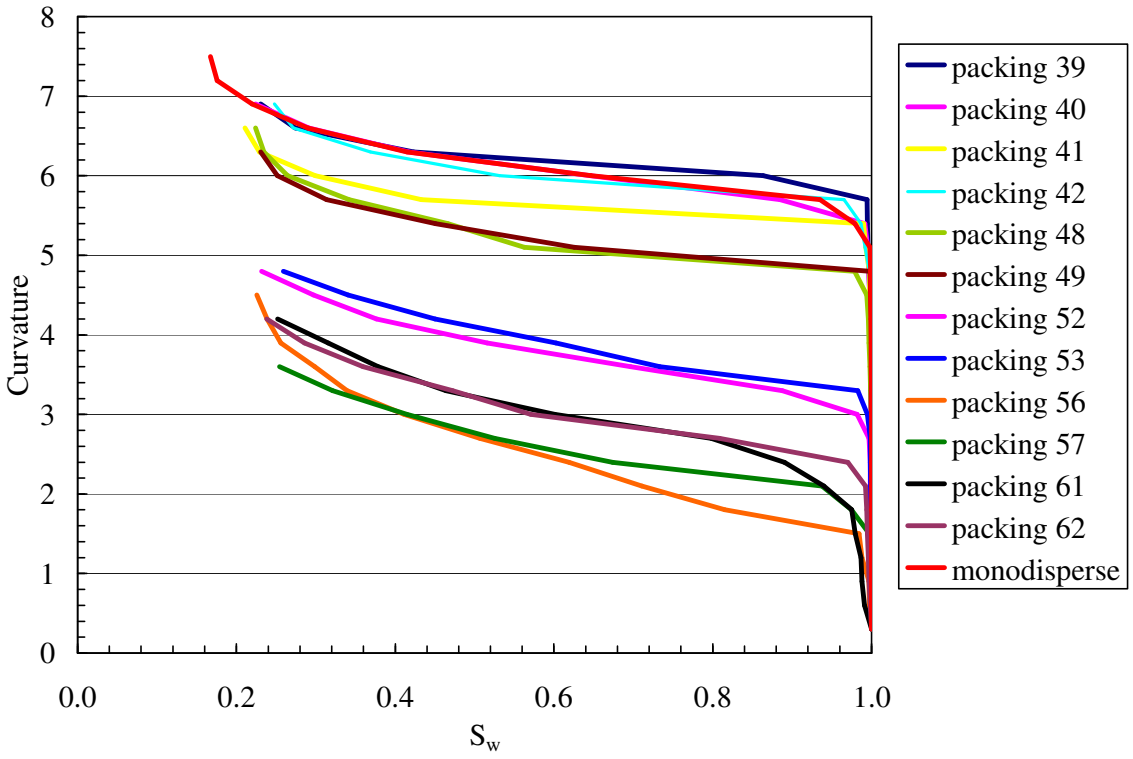

Figure 7. Drainage curves for model sediments, with properties shown in Table 1. The curvature for each sediment is normalized by the mean grain radius. As the grain size distribution in the sediment becomes broader, the pore throat size at which drainage begins becomes smaller. The irreducible wetting phase saturation at the drainage endpoint is similar for all the sediments. Monodisperse packing curve (all radii equal) is added for comparison.

Table 1. Summary of Properties of Different Packings

Packing Number	Mean Radius	Standard Deviation	Porosity	Sorting coefficient $\sqrt{d_{75}/d_{25}}$ (number fraction basis)
39	2.19	0.07	0.34	1.02
40	2.19	0.07	0.35	1.02
41	2.17	0.07	0.38	1.02
42	2.19	0.07	0.37	1.02
48	2.01	0.66	0.33	1.25
49	2.01	0.67	0.34	1.25
52	1.85	0.91	0.34	1.42
53	1.86	0.89	0.35	1.40
56	1.71	1.05	0.31	1.64
57	1.71	1.05	0.35	1.62
61	1.77	1.00	0.31	1.53
62	1.76	1.00	0.35	1.53

The implication of these results is that relatively small changes in the width of the grain size distribution of a sediment are important. Increasing the width, or going to more poorly sorted sediments, enables a gas phase to drain the sediment at considerably lower pressures. In our simulations, moderately and well sorted sediments ($S_o > 1.2$) drain at a dimensionless curvature (and therefore dimensionless capillary pressure) between 2 and 3, while extremely well sorted sediments ($S_o < 1.1$) drain at a dimensionless capillary pressure between 5 and 6. If the pressure required for fracturing the sediment does not depend strongly on the grain size distribution, then the competition between drainage and fracturing could lead to quite different behavior for gas invasion of sediments with different sorting.

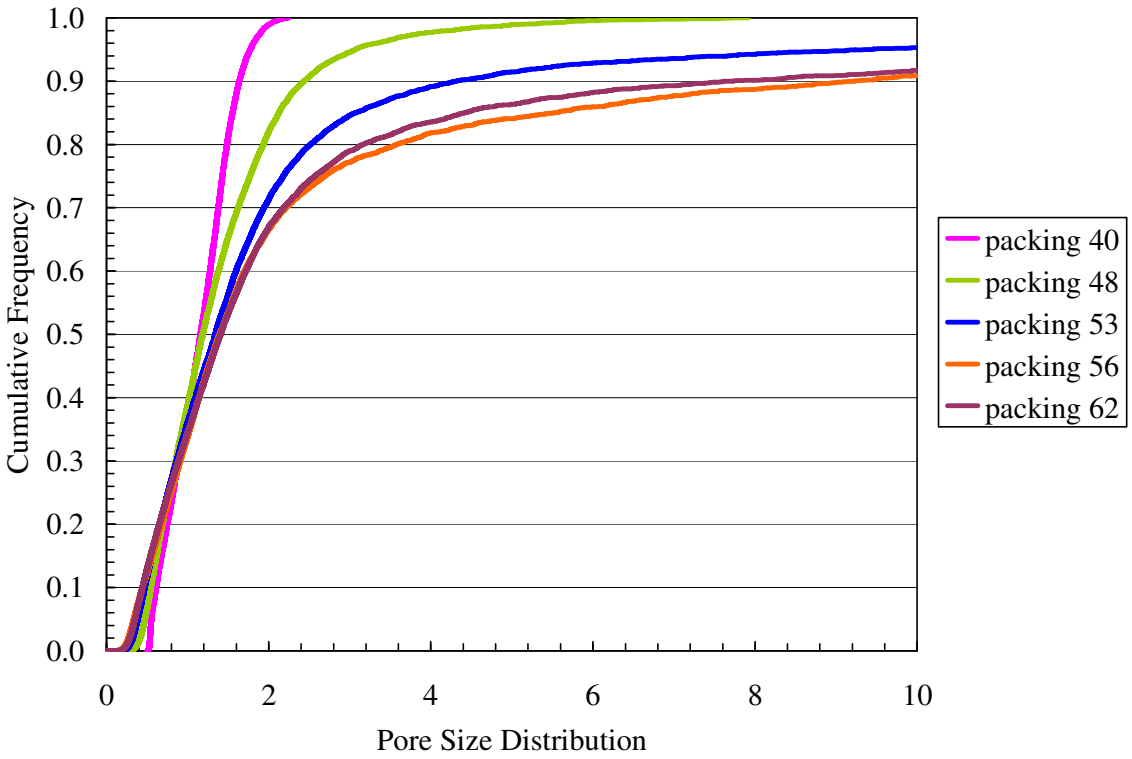

Figure 8. Percolation threshold for drainage in packings of monodisperse spheres is known to be 50% (Bryant et al, 1996). This threshold is still approximately valid for model sediments with broader grain size distributions. The threshold is reached at larger dimensionless pore throat sizes in sediments with broader grain size distributions. Thus drainage occurs in these sediments as smaller capillary pressures, Figure 7.

Effect of Sorting on Irreducible Wetting Phase Saturation

The change in grain size distribution has little effect on the irreducible wetting phase saturation. The average value is 19% (compare to 16.75% for monodisperse packing). Thus sorting will affect whether gas invasion occurs by drainage or by fracturing, but if drainage occurs, the sorting is unlikely to affect nature and distribution of the gas/water interface. Thus we expect similar hydrate growth habit in drained sediments, at least for the range of sorting considered here.

Variation in Connectivity of Wetting Phase Associated with Gas-Water Interfaces During Drainage

The growth of hydrate at the gas/water interface will depend on how much water and gas are available locally and on how much the chlorinity builds up in the available water. The value of $S_{w,irr}$ and the spatial configuration of that water will thus affect the predicted growth habit. A key quantity to be extracted from our simulations is the fraction of the wetting phase that is disconnected from the bulk (connected, percolating) wetting phase as drainage proceeds. Given that growth rates are likely to be proportional to gas/water interfacial area, it is important to determine how much interfacial area is associated with volumes of disconnected wetting phase. Hydrate growth will be limited by water availability in these volumes. Dissolved species such as chloride do not enter the hydrate lattice and will build up on the aqueous phase as hydrate forms. This lowers the melting point of hydrate and can limit growth. If the interface is associated with a percolating cluster of brine-saturated pores, accumulated chlorinity can diffuse from the gas/water interface toward the bulk brine phase. Figure 9 shows the fraction of interfacial area associated with connected water for four packings with Trask sorting coefficients of 1.00 (monodisperse), 1.07 (packing 6), 1.14 (packing 10) and 1.31 (packing 18).

We may summarize these observations in terms of factors limiting hydrate growth as sketched in Figure 10. Nearly all the water is part of the percolating cluster (red curve) during the early stages of drainage. The total area of gas/water interfaces (blue curve) increases steadily during this period. Because both phases (gas and water) are well connected, we expect that hydrate growth would not be limited by availability of CH_4 nor of H_2O. Some other process such as the dissipation of the heat of fusion of the hydrate is likely to be limiting.

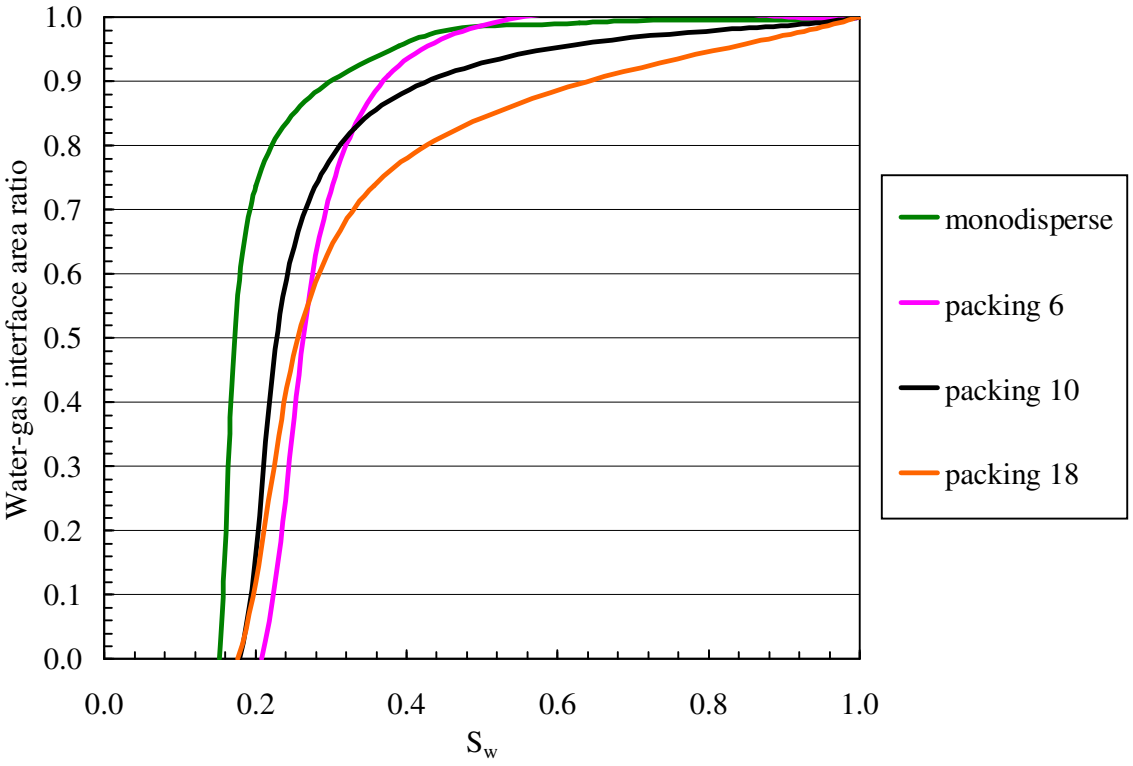

Figure 9. Trask sorting coefficient increases for monodisperse, 6, 10 and 18, in that order. The interface area ratio shown is a ratio of non-trapped water/gas interface area and the total water/gas interface area. The effect of the broader grain size distribution on wetting phase connectivity becomes pronounced for packing 18. The fraction of gas/water interfaces on a percolating cluster of pores containing wetting phase starts to decrease earlier during drainage (at larger values of S_w).

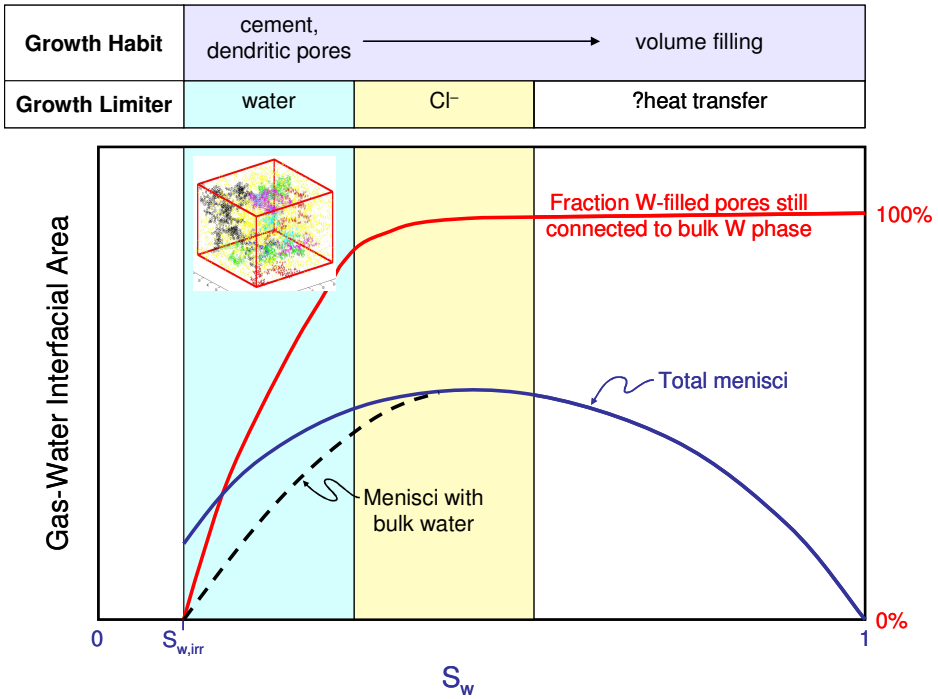

Figure 10. Schematic of connectivity of gas/water interfaces to bulk water during drainage of a sediment. The growth habit and limiting factor for growth are likely to vary with saturation because the spatial distribution of the water phase varies dramatically with saturation. Total gas/water interfacial area is not a monotonic function of saturation.

As drainage proceeds through an intermediate range of saturations, the water phase remains well connected (red curve). However, the percolating cluster is becoming increasingly ramified (dendritic), so that the pathway from a typical pore to the backbone of the cluster is becoming longer and more tortuous. The diffusive transport of excess Cl^- is slower along such paths. Thus the continued growth of hydrate is likely to be limited by the rate of chlorinity transport in this region. As hydrate growth blocks some pore throats, it is likely to block chloride transport. This raises the possibility of co-existing gas, water and hydrate phases in sediments that have been moderately drained. The possibility would be greater in sediments with broader grain size distributions.

As drainage proceeds to smaller water saturations, there is a rapid decline in the fraction of wetting phase that is still connected to the percolating cluster (red curve). The total gas/water interfacial area begins to decrease (blue curve), and the number of gas/water menisci associated with the percolating cluster of water phase decreases even faster (dashed black line). Thus when invading gas has drained a sediment well, we anticipate that hydrate growth at gas/water interfaces will be limited by water availability. The co-existence of a gas phase with the hydrate is therefore likely in drained sediments.

LSM/PQS Results for Stationary Grains

Figure 11 outlines the progression of the algorithm on a simple 2D medium that can be viewed either as a fracture in a sediment or a few pores and throats arranged in a linear fashion. The algorithm captures essential reversible and irreversible behavior: Haines jumps in throats (between sphere pairs (A,B), (C,D) and (E,F)) as well as Melrose criterion for pore imbibition (instability caused by different fluid menisci coming into contact). Figure 12 shows the corresponding drainage and imbibition curves.

Note that our simulations establish the exact position and shape of the interface in porous geometries, from which fluid volumes, contact areas and interface curvatures can be obtained.

We further tested the algorithm on a (3D) subset from a close packing of equal spheres measured by Finney (1970). The pore-grain interface of the subset is shown in Figure 13a, and a drainage endpoint where the non-wetting fluid percolated the packing is shown in Figure 13b. Figure 13c shows one of the final stages in drainage simulation where the wetting phase in the accessible part of the pore space is present almost exclusively in the form of pendular rings around sphere contacts. Figure 14 shows the curvature-saturation relationship for the entire drainage and imbibition sequences as well as their favorable comparison to Haines' experiment.

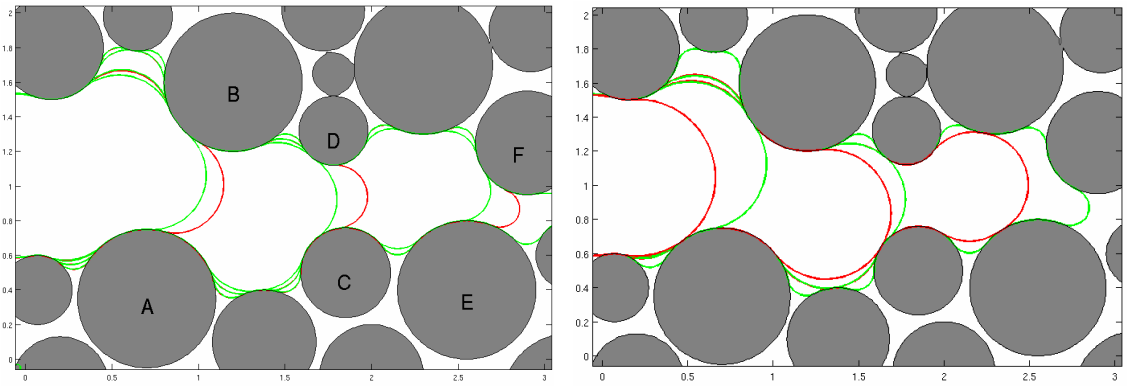

Figure 11. Selected fluid-fluid interface positions in a 2D model fracture at drainage (right) and imbibition (left). Starting fluid-fluid interface is shown in green in both figures. During drainage, the meniscus advances from left to right as the applied curvature increases, and from right to left as applied curvature decreases during imbibition. Positions before and after Haines jumps at drainage (left) and before and after individual pore imbibitions (right) follow in alternating red and green colors.

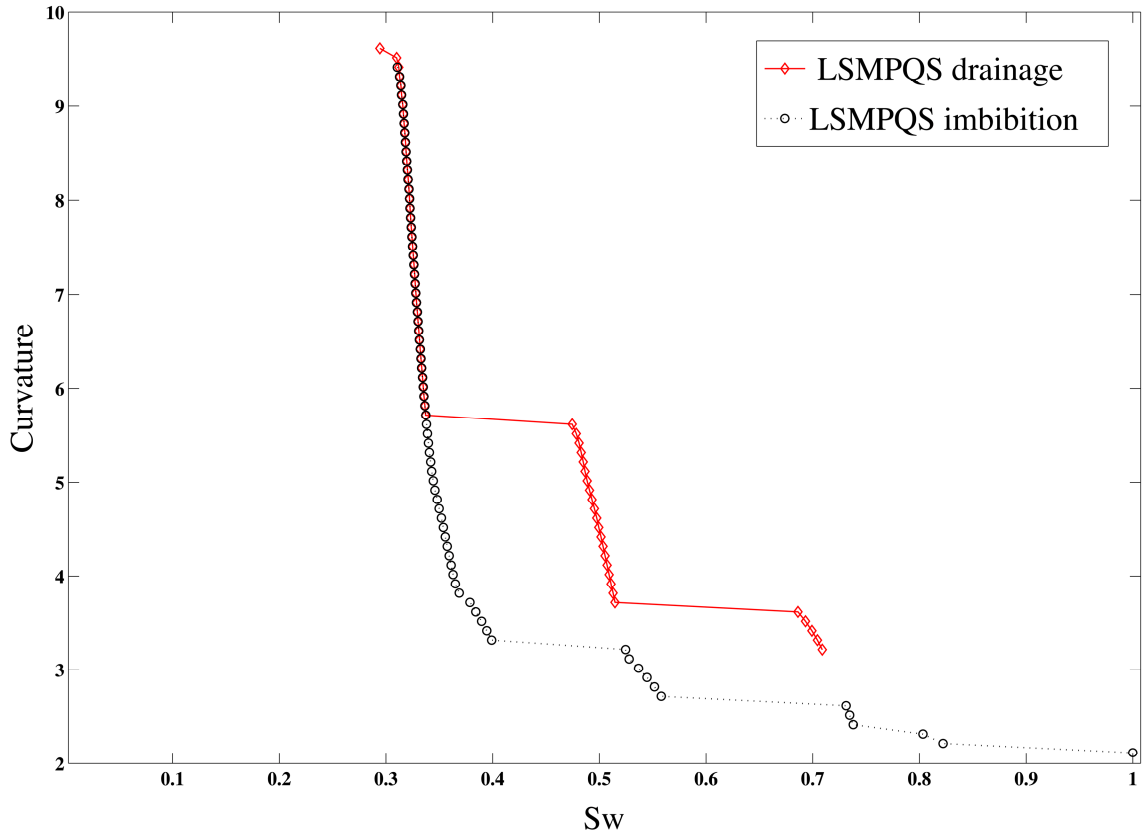

Figure 12. Curvature-wetting fluid saturation plot for drainage and imbibition of the two dimensional fracture in Figure 11. The jumps in the plot correspond to Haines jumps during drainage and to withdrawal of non-wetting phase from an individual pore during imbibition. Withdrawal occurs when the Melrose criterion is satisfied, that is, when two distinct menisci come into contact on a grain surface.

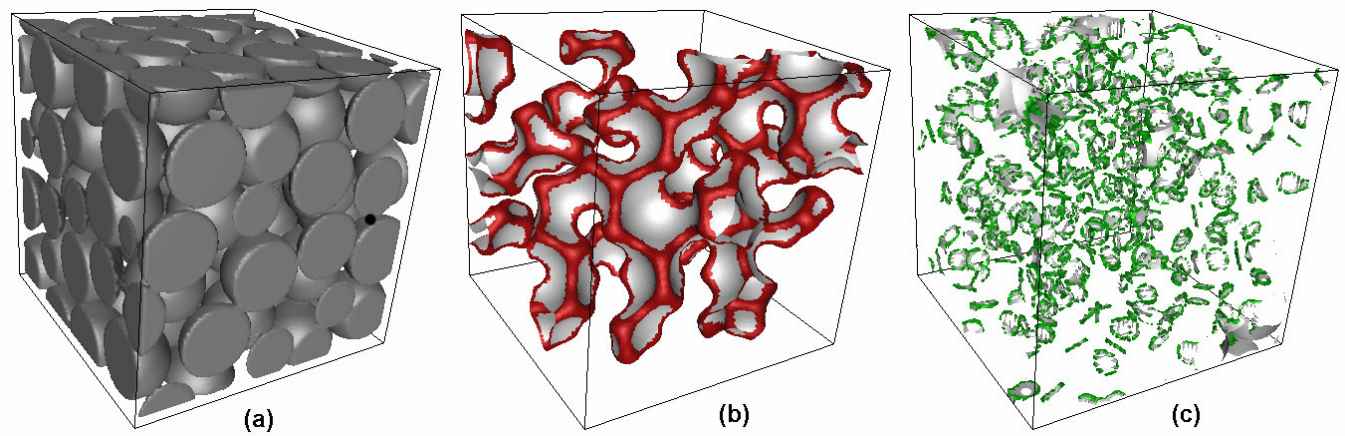

Figure 13. (a) Pore-grain surface of 75 spheres from the Finney packing. Sphere have radius R=1.0, and for simulation purposes they were discretized at dx=0.08, creating a 100^3 sample. (b) Drainage simulation (LSM/PQS algorithm) starts from the face in the back, and the plot shows the non-wetting fluid surface at the drainage endpoint where it percolates to the opposite face. The part of the surface in contact with the wetting fluid is shown in red, and the part in contact with solid is shown in gray. (c) Wetting fluid surface (fluid-fluid part in green, fluid-solid part in gray) corresponding to a curvature near the end of simulation. At this curvature, wetting fluid is mostly in the form of pendular rings.

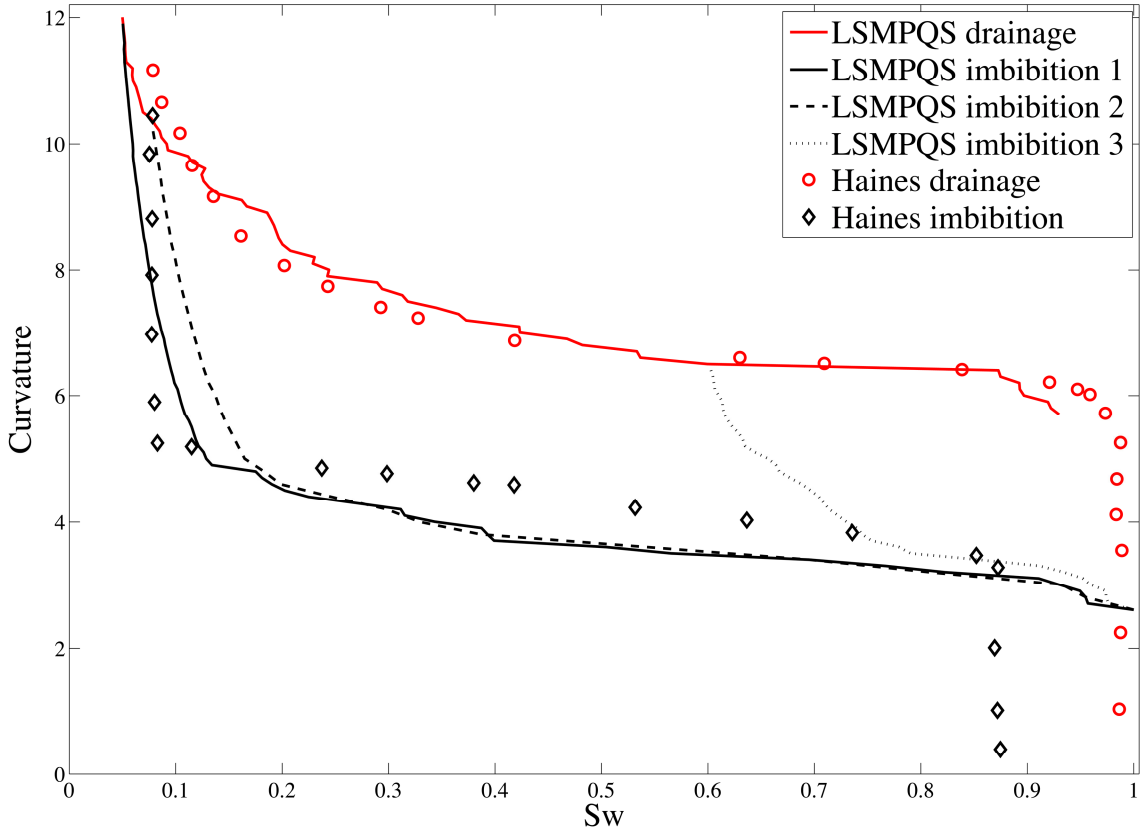

Figure 14. Comparison of LSM/PQS drainage and three different imbibition simulation curvature – saturation curves with an experimental data in a packing of equal spheres by Haines (1930). This is a small sample, and all volume edge boundaries were open to flow, so LSM/PQS shows no trapped non-wetting phase. The algorithm can capture snap-off and the resulting trapping, as shown in Prodanović and Bryant (2008).

DEM Results of Coupled Poromechanics with Single Fluid Phase

In this section we present some of the simulations for the validation of the coupled fluid-micromechanical model. This is a necessary step to build confidence that all the important mechanisms that play a role in methane gas migration (in particular, those related to fracturing) are properly captured. The validation of the model included:

1) *Isochoric pressurization tests* that must reproduce wall loading (Figures 15 and 16). We illustrate the importance of bond strength with an isochoric pressurization test (see Figure 15). The fluid pressure is ramped up in stages, uniformly for all pores in the sediment sample. In Figure 16 we show the evolution of the associated increase in wall stress as a function of fluid pressure, for a consolidated rock that supports tension between grains ("tension"), and a granular material that does not ("no tension"). The difference is apparent, and it reflects the micromechanical mechanism of bond failure which, in turn, may greatly affect the hydraulic properties of the medium.
2) Multistep inflow/outflow test that must capture pressure transients, as well as pore volume changes and pore-to-pore flow (Figure 17). In this test, the pores near the top boundary are pressurized in stages. The hydraulic response of the rest of the pores in the sample is recorded, and this is shown in Figure 17. At a pore in the middle of the domain, the pressure follows the pressure at the boundary, but with a lag due to the time required for the pressure to diffuse through the pore throats. After each pressurization stage, the net inflow into this pore increases, then decreases to zero as the system relaxes to a new steady state. Due to pressurization of the sample, the pore volume also increases in stages, as the grains are pushed towards the fixed boundary.
3) Uniaxial pressurization tests that must reproduce the pressure diffusion across the fluid network (Figure 18). In this test, the pressure at the top boundary is increased suddenly. The pressure increases in the granular sample, following a diffusive process. In Figure 18 we plot the cross-section averaged pressure at different times, which simulate this diffusive process towards the steady state. Simple curve fitting would allow one to obtain the effective permeability of the sample.
4) Drained consolidation tests that must predict the macroscopic diffusive behavior of the pressure transient, as well as stress-strain curves governed by the effective stress (Figure 19). This type of simulation allows one to obtain the macroscopic elastic and poroelastic parameters corresponding to the grain-scale model.

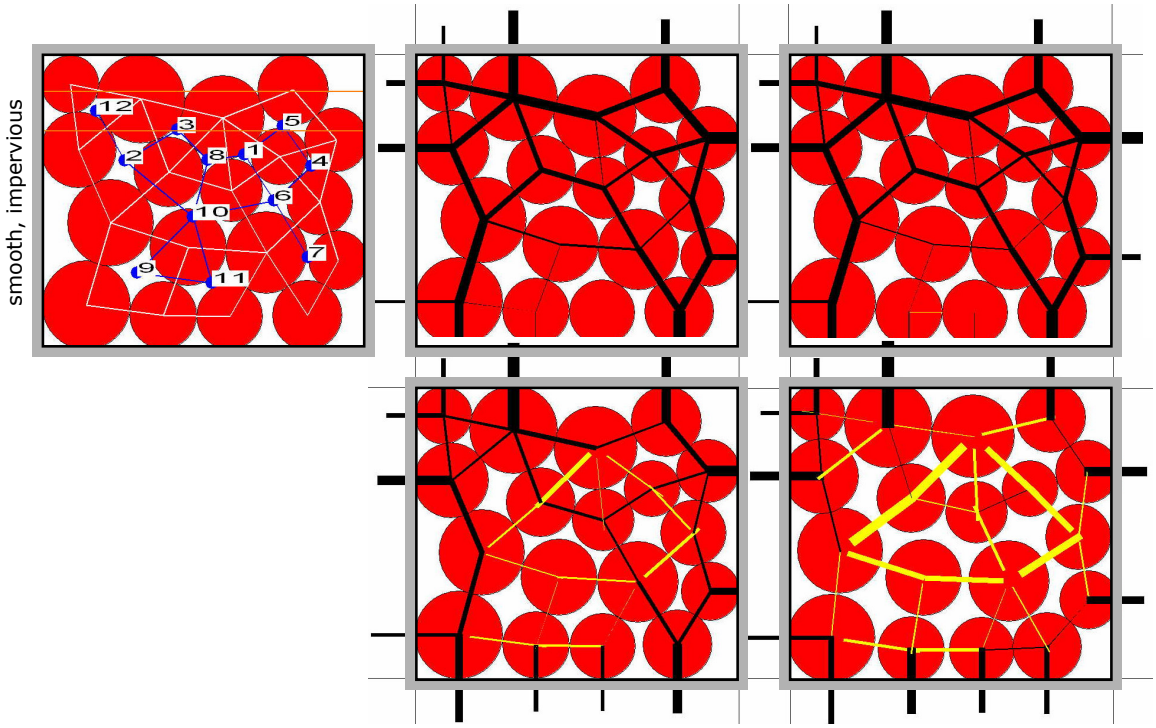

Figure 15. Wall loading during an isochoric pressurization test.

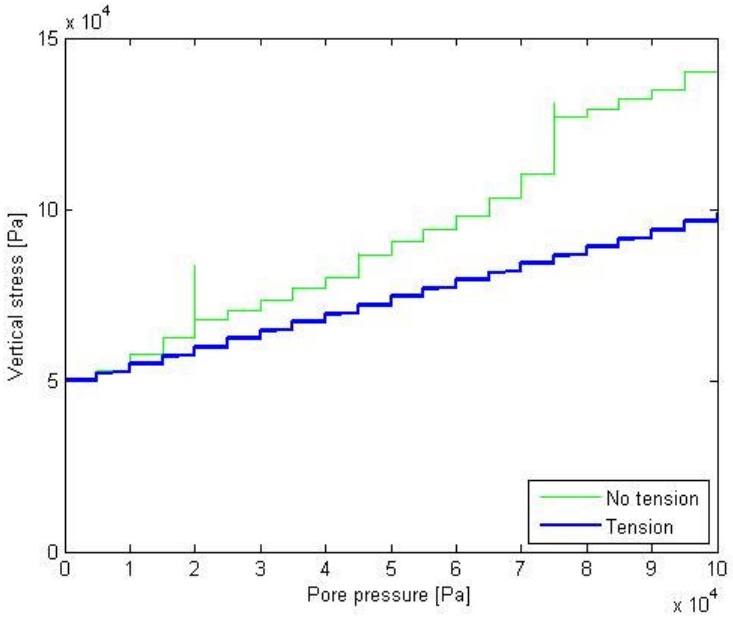

Figure 16. Wall stress in an isochoric pressurization test for a consolidated material ("tension") and a granular material ("no tension").

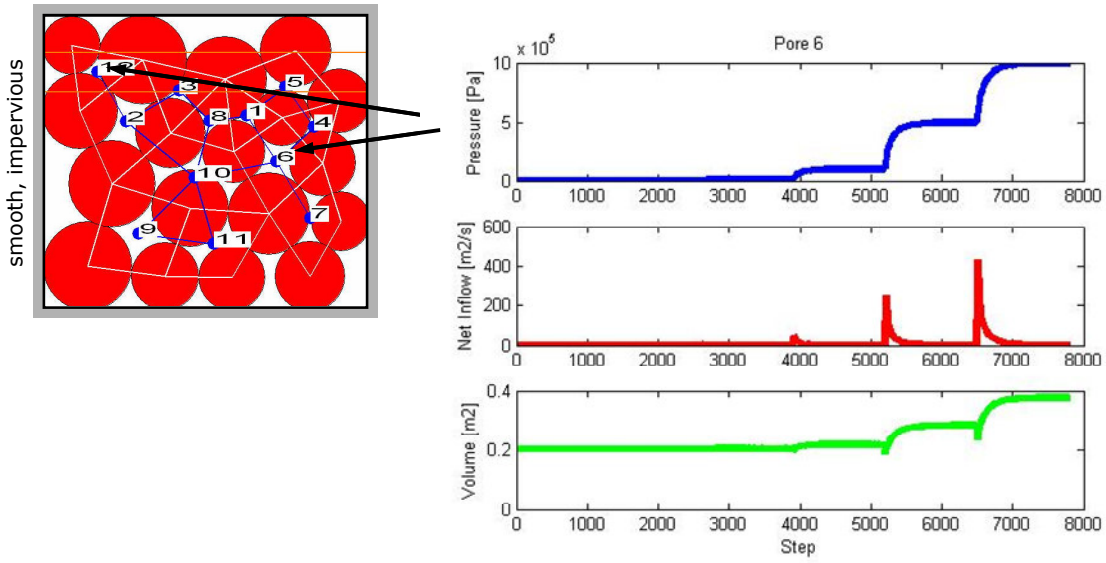

Figure 17. Pressure evolution, pore-to-pore flow, and pore volume at individual pores in a multistep pressurization test. The pressure is increased in stages at pore 12, and the response is recorded at pore 6 (arrows on the left figure indicate pores in question).

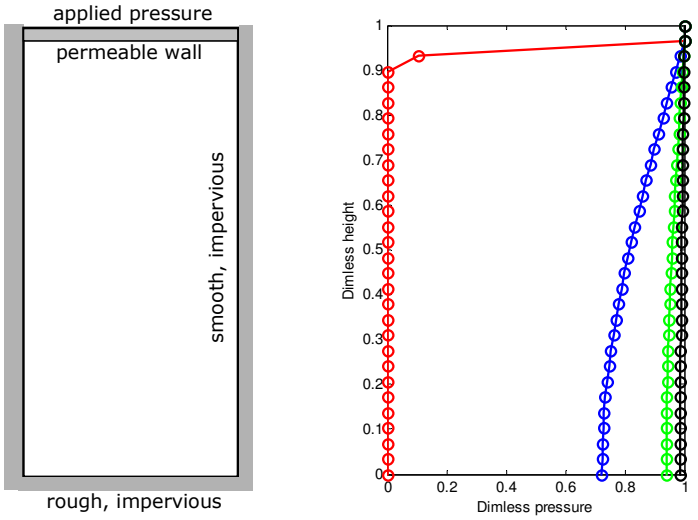

Figure 18. Width-averaged evolution of the pressure in a one-dimensional pressurization test.

DEM Results of Coupled Poromechanics with Two Fluid Phases

The developments briefly described above now permit investigating the poromechanical behavior of model sediments under a variety of scenarios. Of particular interest is the influence of bonding between grains, and the dependence of the mechanical deformation on the strength of those bonds. The model now allows one to investigate under which conditions the material will "fracture" (the fluid pressure is sufficiently high that bonds will break under tension). By resolving the dynamics of the flow and the texture (layering) of the sediment, we can also investigate whether failure will be isotropic or in a preferential direction. While these issues have been investigated at length for dry media, their characterization for fluid-saturated media (especially, when two fluids are present) is still an open issue.

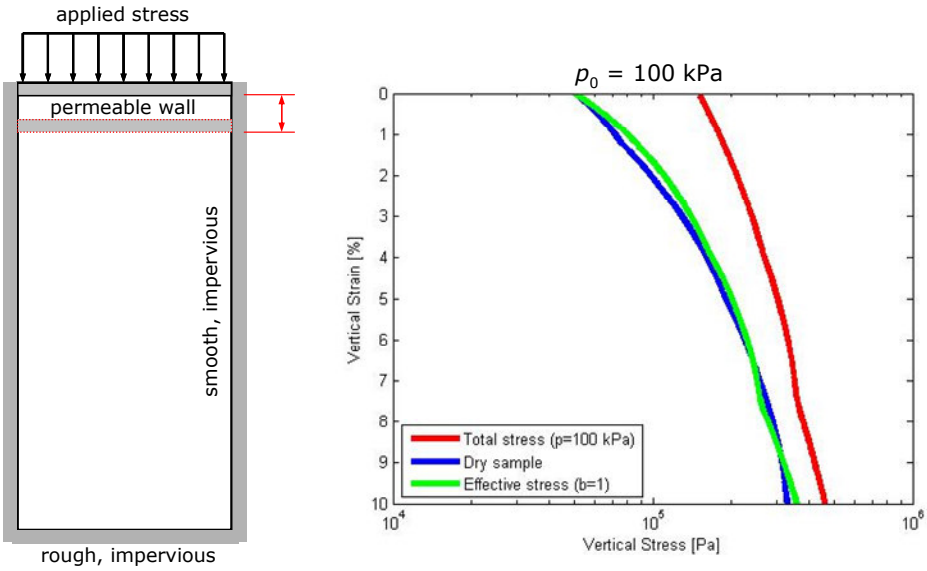

Figure 19. Stress-strain curves (total stress and effective stress) for a one-dimensional consolidation test.

We are particularly interested in the simulation of sediment fracturing upon invasion of a second fluid phase. In a two-fluid system, the difference in pressures between the fluids does not diffuse or equilibrate, due to surface tension effects. As explained earlier, we adopt an "elastic membrane" representation of the gas/water interface that only allows normal forces to be transmitted. Adhesion forces are neglected at this stage. When the bond between two grains is lost, the "membrane" advances and a new pore is loaded with a higher pressure. By choosing the parameters of the hydraulic conductance appropriately, we can model the advancement of the fluid-fluid interface and, correspondingly, the changes in pore pressure. We find that, under most scenarios, this leads to fracturing of the medium. This is shown in Figure 20.

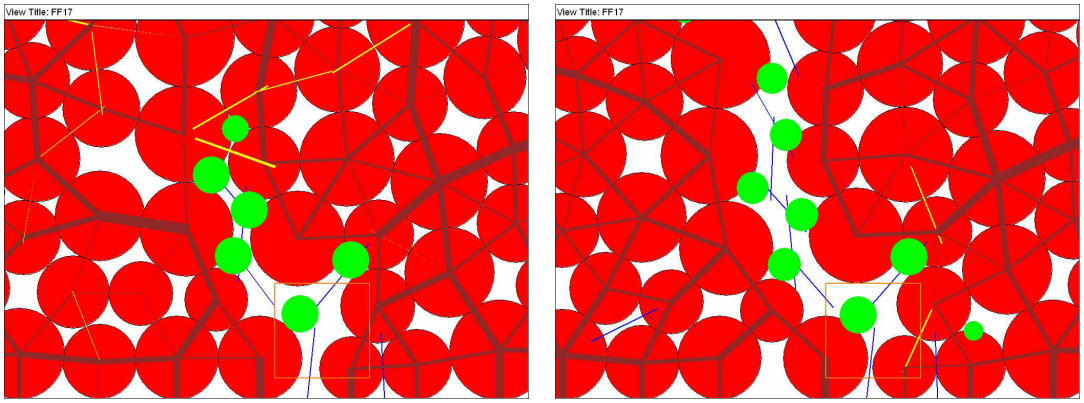

Figure 20. Illustration of fracturing of the sediment due to invasion of a gas phase into a brine-saturated sediment. The green dots represent the pores that have been invaded by gas. Gas and brine pressure are different due to the surface tension effects. This example is representative of the typical behavior observed numerically for the mechanical behavior of granular materials under fluid-fluid displacements.

In many (passive) depositional environments, the horizontal stress is lower than the vertical stress. In such scenarios, one expects the development of vertical fractures that open up the sediment in the direction of minimum compressive stress, and the conceptual picture shown in Figure 20 is relevant. In Figure 21 we show that fracturing of the sediment is not necessarily restricted to anisotropic Earth stresses. Even when horizontal and vertical stresses are equal, the medium tends to fracture in a set of radial, geometrically complex fractures, if gas is injected into a brine-saturated sediment.

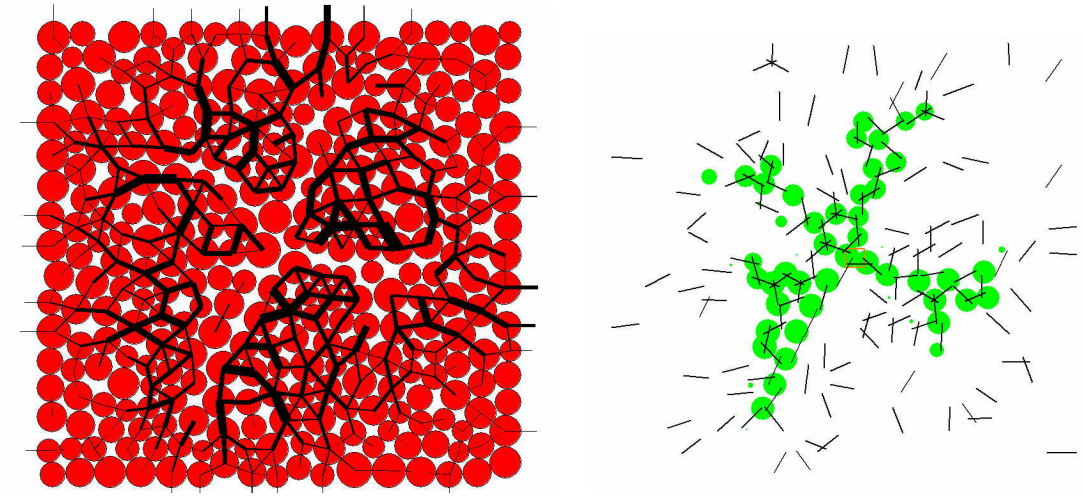

Figure 21. Illustration of the fracturing behavior of a model sediment upon injection of gas, when the vertical and horizontal stresses are equal. The sediment fractures "isotropically" into a set of radial, geometrically-complex fractures.

LSM/PQS Results for Drainage Coupled with Grain Displacement

It is instructive to compare these simulations, which are rigorous for capillary forces but not grain mechanics, with those of the previous section, which are rigorous for grain mechanics but not capillary forces. We illustrate the coupled behavior in two 2D packs of circular grains. The first one was obtained by packing disks of unit radius on a regular triangular grid except for one disk that was slightly offset (see Figure 22). Drainage curves (Figure 23) show remarkable qualitative and quantitative differences for this simple medium due to coupling of fluid and sediment movement. In the case of stationary grains (not shown), almost all the pore throats are the same size and thus almost the entire domain drains quite suddenly when the applied curvature increases to 11. When fluid pressure displaces the grains, Fig. 22, the domain begins to drain at much smaller curvatures, the percolation threshold is much less sharp, and the irreducible wetting saturation is larger. The first of these three observations makes intuitive sense: moving grains apart decreases the critical curvature required to force a meniscus between them. Less obvious are the second and third observations. Behind the advancing gas phase, grains are pushed into each other, narrowing the pore throats between them. This increases the pressure required to invade the undrained region behind the leading edge of the advancing front. Thus the drainage curve is smoothed out in the coupled displacement.

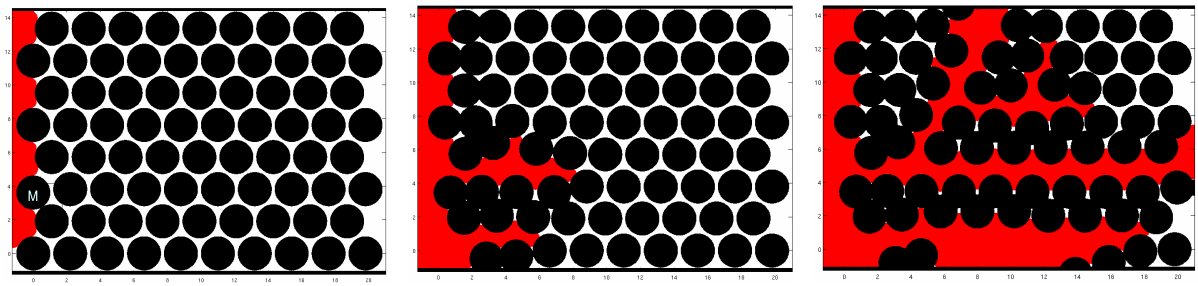

Figure 22. (Left) NW fluid at the first step of PQS simulation is shown in red, C=2.36. The spheres (in black) form a regular packing (except for one sphere in the first column – marked by letter M - that is offset slightly) and have not moved yet. (Center) NW fluid at C=6.36 of the coupled PQS simulation. The packing "irregularity" has, under coupled fluid and sediment movement, triggered an opening of two fluid pathways. (Right) Fluid/sediment configuration at the point where fluid percolates to the other side (C=8.56).

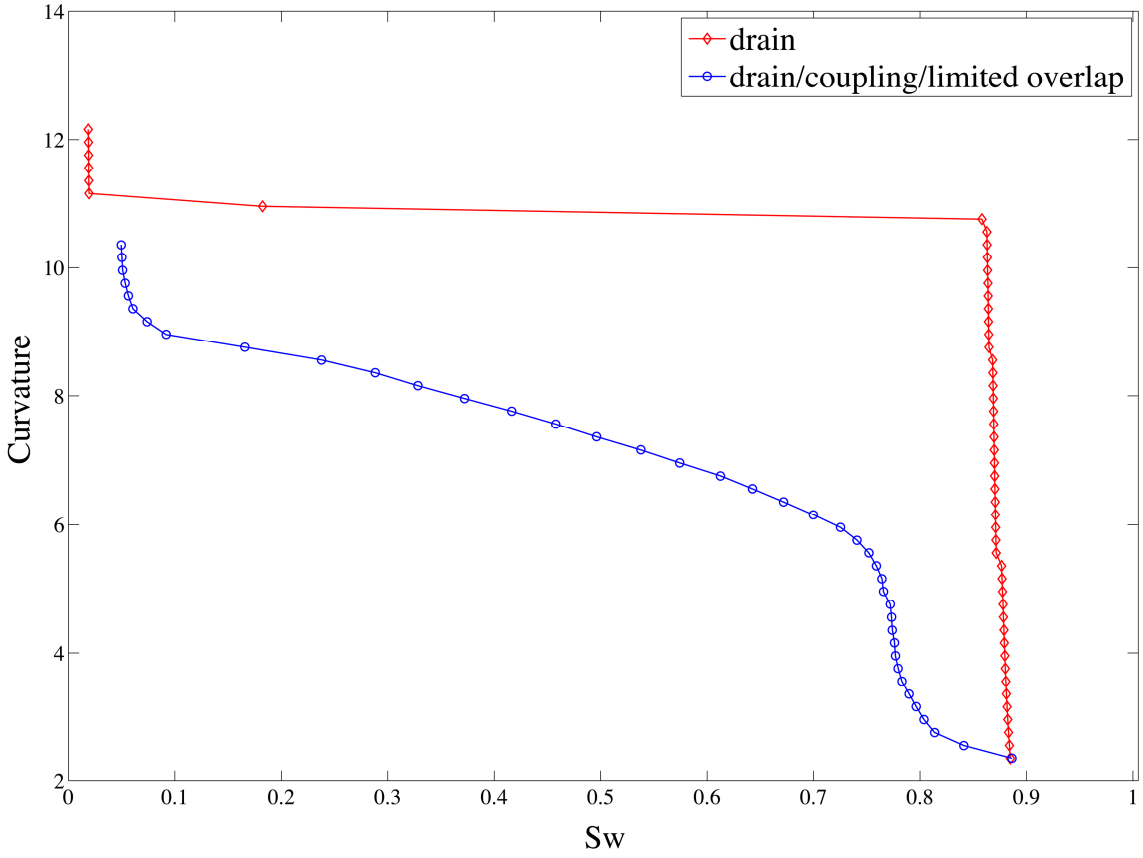

Figure 23. Comparison of curvature-wetting fluid saturation curves for drainage in the regular packing of disks with and without coupling. Note that the initial packing has basically only two throat sizes. Thus if the grains are stationary, once curvature is high enough to drain the smaller throats, the whole rest of the domain drains. This yields a characteristic single large jump in the corresponding C-Sw curve.

The second geometry is a cross-section of the Finney pack resulting in a close packing of disks with radius 1.0 or less (Figures 24 and 25). We removed three disks at the entrance to create a preferred region for onset of grain displacement. The displacement becomes self reinforcing: moving grain decreases the curvature required for drainage to occur, leading to gas invasion that moves grain apart in the invaded pore.

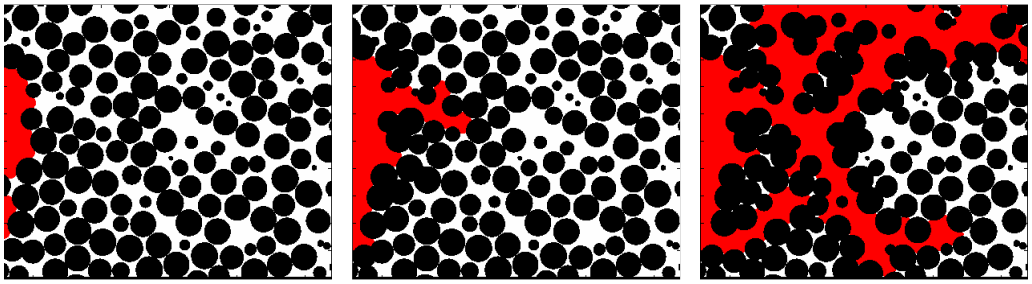

Figure 24. (Left) NW fluid at the first step of PQS simulation is shown in red (C=2.48). The spheres (in black) have not moved yet. (Center) NW fluid at C=3.68 of the coupled PQS simulation. The fluid has opened a pathway, which just started to split into two. (Right) Fluid/sediment configuration at C=6.08 where fluid percolates to the other side for the first time.

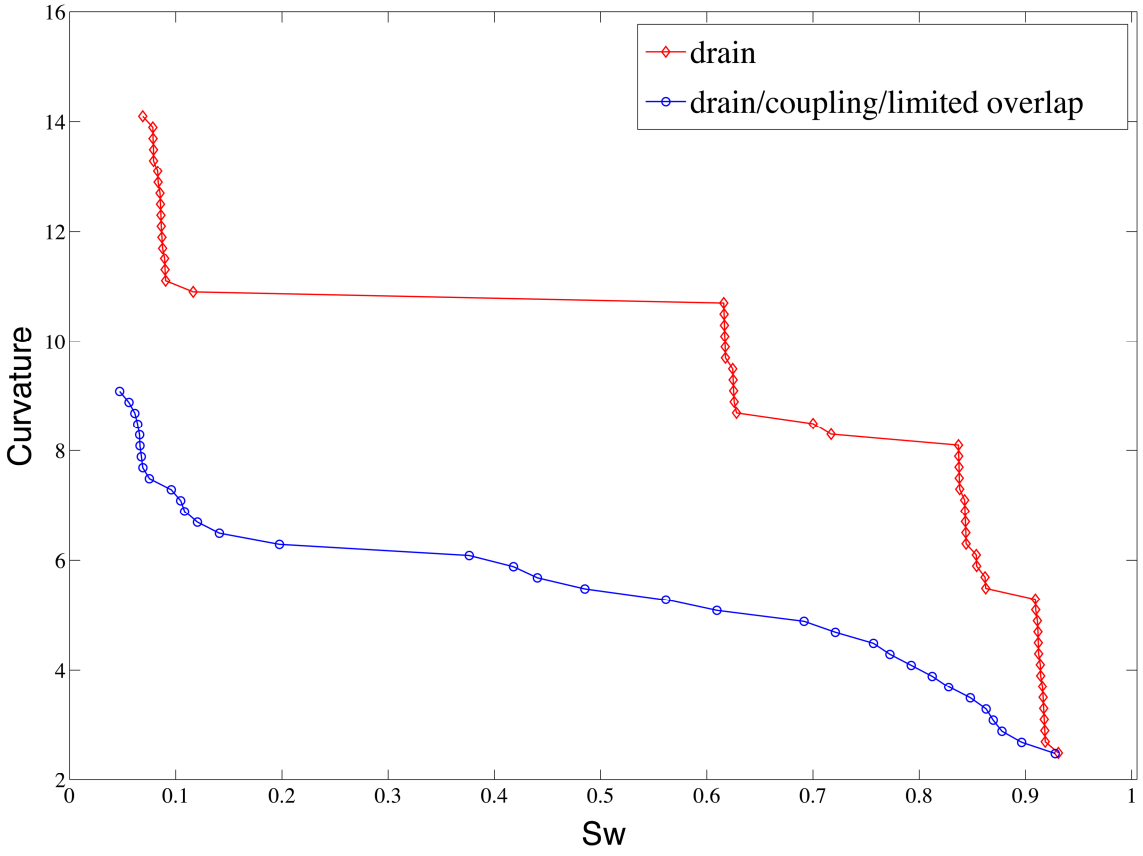

Figure 25. Comparison of curvature-wetting fluid saturation curves for drainage in the regular packing of disks with and without coupling.

The coupling implemented above is not physically rigorous. Nevertheless it shows that the fluid and granular movement can be successfully put together. More importantly, the physical character of the drainage displacement changes. Coupling with the physically correct granular movement (simulated via DEM) will be slightly more involved (due to different software/platforms) and is part of the future work.

Conclusions

We have developed several methods useful in examining the role of gas phase invasion of the hydrate stability zone. These methods apply to the two limiting cases of invasion by drainage (capillarity controlled) and invasion by fracture propagation (grain mechanics controlled).

To study the limiting case of capillarity-controlled invasion, we conducted drainage simulations in infinite-acting, physically representative network models of sediment pore space. The networks are extracted directly from the grain space of a series of model sediments, dense random packings of spheres of various size distributions. This approach eliminates boundary effects common to finite networks and thus should provide a more realistic estimate of water distribution in drained sediments.

The simulations show three regimes of gas-water configuration: at large saturations of water, both water and gas phases are well connected; at intermediate water saturations, the water remains connected to the bulk but through longer and more tortuous paths; at small water saturations, the water is increasingly disconnected. This suggests that hydrate growth would not be limited by supply of H_2O or CH_4 molecules in the at large S_w; at intermediate S_w hydrate growth would be constrained by the rate at which salinity (chloride anions) could diffuse from the interface to the bulk; at small S_w hydrate growth would be constrained by availability of H_2O molecules. We therefore expect that gas, brine and hydrate phases are likely to co-exist in sediments that have been moderately to well drained (invaded) by gas phase. The simulations also show that the total area of gas-water interface is maximum at intermediate S_w, but the fraction of menisci associated with bulk (connected) water decreases rapidly as S_w decreases. Consequently the overall rate of methane hydrate growth will not exhibit a simple dependence on S_w.

We have applied a progressive quasi-static (PQS) algorithm based on a level set method for interface tracking to simulate drainage and imbibition directly in a subset (ca. 100 spheres) of the model sediments. The predicted capillary pressu-saturation trends agree with experiments. This establishes a basis for determining gas-water interfaces in geometries for

which the network approach is less well suited, e.g. in rough-walled fractures formed by gas invasion and in sediments with a broad distribution of grain sizes.

We have extended the discrete element method (DEM) to model the coupling between the pore fluids and the solid and thereby predict the onset of sediment fracturing by gas phase pressure under in situ loading conditions. The DEM grain mechanics model reproduces the key processes in the fluid-solid interaction by accounting for the different pressure of brine and methane gas, in a "membrane" two-fluid model. It was validated by means of isochoric pressurization tests, multistep inflow/outflow experiments, drained/undrained consolidation tests, and it reproduces the sediment stress-strain behavior in laboratory triaxial experiments. The DEM model shows that fracturing of the sediment is favored in fluid-fluid displacements through poorly-consolidated material.

To examine qualitatively the behavior emerging from competition between fracture propagation and drainage, we implemented a simple kinematic model of grain displacement during gas phase invasion of a sediment. The PQS algorithm was modified so that grains touching the gas-water interface are moved a short distance. The nature of the resulting displacement can be much different than when the grains are fixed. We presented two simple, coupled models with different emphases (one on the fluid displacement, one of the poro-mechanics). Despite their simplifications, both models indicate that mechanical effects are essential to capture the essential pathways for gas migration into a soft sediment. Work is under way to merge the DEM and the PQS codes into a single simulation environment.

Acknowledgements

The authors are grateful to the Department of Energy (DE-FC26-06NT43067) for supporting this research.

References

Al-Raoush, R., K. Thompson, and C. S. Willson (2003). Comparison of Network Generation Techniques for Unconsolidated Porous Media. Soil Sci. Soc. Am. J. 67: 1687-1700.

Behseresht, J., S. L. Bryant, and K. Sepehrnoori (2007), Infinite-Acting Physically Representative Networks for Capillarity-Controlled Displacements, SPE110581 prepared for SPE ATCE 2007, Anaheim, CA, November 2007

Bhatnagar, G., W. G. Chapman, G. R. Dickens, B. Dugan and G. J. Hirasaki (2007), Generalization of gas hydrate distribution and saturation in marine sediments by scaling of thermodynamic and transport processes. Am. J. Sci. 307:861-900.

Biot, M. A. (1941), General theory of three-dimensional consolidation. J. Appl. Phys., 12:155–164.

Bruno, M. S. (1994). Micromechanics of stress-induced permeability anisotropy and damage in sedimentary rocks. Mech. Mater., 18:31–48.

Bruno, M. S. and R. B. Nelson (1991). Microstructural analysis of the inelastic behavior of sedimentary rock. Mech. Mater., 12(2):95–118.

Bryant, S., Mason, G., and Mellor, D. (1996), "Quantification of Spatial Correlation in Porous Media and Its Effect on Mercury Porosimetry," Journal of Colloid and Interface Science, Vol. 177, pp.88-100.

Bryant, S., Mellor, D., and Cade, C. (1993) "Physically Representative Network Models of Transport in Porous Media," American Institute of Chemical Engineers (AIChE) Journal, Vol. 39, No. 3, pp. 387-396.

Chu, K.T. and M. Prodanović: Level Set Method Library (LSMLIB), http://www.princeton.edu/~ktchu/software/lsmlib/

Cook, B.K., D. R. Noble, and J. R. Williams (2004). A direct simulation method for particle-fluid systems. Eng. Comput., 21(2–4):151–168.

Cundall, P. A. and O. D. L. Strack (1979). Discrete numerical model for granular assemblies. Geotechnique, 29:47–65.

Fatt, I. (1956a). "The Network Model of Porous Media I. Capillary Pressure Characteristics." Trans Soc. Min. Eng. AIME 207: 144-159.

Fatt, I. (1956b). "The Network Model of Porous Media II. Dynamic Properties of a Single Size Tube Network." Trans Soc. Min. Eng. AIME 207: 160-163.

Fatt, I. (1956c). "The Network Model of Porous Media III. Dynamic Properties of Networks with Tube Radius Distribution." Trans Soc. Min. Eng. AIME 207: 164-181.

Finney, J.L. (1970): "Random Packings and the Structure of Simple Liquids I: The Geometry of Random Packings," *Proc. Royal Society of London* 319:479.

Haines, W. B. (1930). Studies in the physical properties of Soil 5. The hysteresis effect in capillary properties and the modes of moisture distribution. J. Agric. Sci. 20: 97.

ITASCA. PFC3D, v3.1 – Theory and Background. Itasca Consulting Group, Inc., Minneapolis, MN, 2005.

Li L. and R.M. Holt (2004), A study on the calculation of particle volumetric deformation in a fluid coupled PFC model. In *Numerical modeling in micromechanics via particle methods -- 2004: proceedings of the 2nd International PFC2D/PFC3D Symposium*, Shimizu, Hart & Cundall (eds). Taylor & Francis Group: London, pp. 273-279.

Lian, G., C. Thornton and M. J. Adams (1993), A theoretical study of the liquid bridge forces between two rigid spherical bodies. J. Colloid Interface Sci. 161:138-147.

Mason, G. and D. W. Mellor (1995). "Simulation of Drainage and Imbibition in a Random packing of Equal Spheres." J. Colloid Interface Sci. 176: 214-225.

Mayer, R. P. and R. A. Stowe (1965). Mercury porosimetry-breakthrough pressure for penetration between packed spheres. J. Colloid Interface Sci. 20: 893.

Orr, F.M., L. E. Scriven and A. P. Rivas (1975). Pendular rings between solids – meniscus properties and capillary force. J. Fluid Mech. 67:723-742.

Osher, S. and R. Fedkiw (2001), Level Set Methods and Dynamic Implicit Surfaces Springer-Verlag.

Princen, H. M. (1969a). Capillary phenomena in assemblies of parallel cylinders I. Capillary rise between 2 cylinders. J. Colloid Interface Sci. 30: 69.

Princen, H. M. (1969b). Capillary phenomena in assemblies of parallel cylinders II. Capillary rise in systems with more than 2 cylinders. J. Colloid Interface Sci. 30: 359.

Princen, H. M. (1970). Capillary phenomena in assemblies of parallel cylinders III. Liquid columns between horizontal parallel cylinders J. Colloid Interface Sci. 34: 171.

Prodanović, M. and Bryant, S.L. (2006) "A level set method for determining critical curvatures for drainage and imbibition," J. Colloid Interface Sci., Volume 304, Issue 2, Pages 442-458.

Prodanović, M. and S.L. Bryant (2007). Physics-driven interface modeling for drainage and imbibition in fractures. SPE110448 prepared for SPE ATCE 2007, Anaheim, CA, November 2007

Prodanović, M. and S.L. Bryant (2008). Resolving Meniscus Movement Within Rough Confining Surfaces Via the Level Set Method. In *Focus on Water Resource Research Trends,* ed. Eetu Haikkinen, Nova Science Publishers, Hauppage, New York. In press.

Sethian, J.A. (1999). Level Set Methods and Fast Marching Methods. Cambridge University Press

Shimizu, Y. (2004), Fluid coupling in PFC2D and PFC3D. In Y. Shimizu, R. D. Hart, and P. Cundall, editors, Numerical Modeling in Micromechanics Via Particle Methods. Proc. of the 2nd International PFC Symposium, Kyoto, Japan, pages 281–287, Balkema, Leiden, October 2004.

Thane, C. G. (2006). Geometry and Topology of Model Sediments and Their influence on Sediment Properties. Department of Petroleum and Geosystems Engineering. Austin, University of Texas at Austin. Masters: 206.

Wilkinson, D. and J. F. Willemsen (1983). "Invasion percolation: a new form of percolation theory." Journal of Physics A. Mathematical and general 16: 3365-3376.

Willett, C. D., M. J. Adams, S. A. Johnson and J. P. K. Seville (2000), Capillary bridges between two spherical bodies. Langmuir 16:9396-9405.